Strongly screening β^- decay antineutrino energy loss in presupernova*

Jing-Jing Liu(刘晶晶)[1)] Dong-Mei Liu(刘冬梅)[2)] Liang-Huan Hao(郝良焕)

College of Science, Hainan tropical ocean University, Sanya 572022, China

Abstract: In this study, we investigate the ion-ball screening model (model (I)), focused on the screening electrostatic potential per electron under the Wigner-Seitz approximation and the Q-value correction. By considering the changes of the Coulomb free energy and the effects of strong electron screening (SES) on the Q-value and the Coulomb chemical potential, we discuss the linear-response screening model (model (II)). We also analyze the influence of the SES on the β^- decay antineutrino energy loss rate by considering the corrections of the Q-value, the electron chemical potential, and electron energy, as well as the shell and pair effects. The antineutrino energy loss rate is found to increase by two orders of magnitude (e.g., the SES enhancement factor reaches 651.9 for model (II)) due to the SES effect.

Keywords: supernovae, evolution, nuclear reactions

PACS: 24.30.-v, 26.20.Np, 26.60.Gj **DOI:** 10.1088/1674-1137/43/6/064107

1 Introduction

The beta decay antineutrino energy loss rates (AELR) of ^{56}V, ^{56}Cr, ^{56}Mn, ^{56}Fe, ^{56}Co, and ^{56}Ni are key parameters in numerical simulation of supernova. The neutrinos and antineutrinos are transparent to the stellar matter and cause stellar core cooling. The neutrino energy loss rates caused by the beta decay and electron capture (EC) in presupernova have been investigated in previous studies (e.g., Fuller et al. [1, 2] (FFN) ; Aufderheide et al. [3, 4] (AUFD); Langanke et al. [5, 6]). In our previous studies [7–9], we have discussed the electron capture and beta decay reactions along with the related issues. The AELR by EC has likewise posed an interesting problem in the investigation of cooling of a neutron star [10–13], because the EC rates could be affected by many factors, such as density of the matter, electron fractions [14–16], temperature, and magnetic field strength, which may in turn influence the equation of state and spin evolution of the star [17-20]. However, all of the studies mentioned above neglected the effect of strong electron screening (SES) on the neutrino energy loss rates.

Some astrophysicists (e.g., studies depicted Refs. [20–26]) discussed the SES problem in detail. Many works (e.g., Refs. [27–30]) also addressed the the effects of ion and electron screening on thermonuclear reaction rates. However, these studies did not consider the influence of SES on the chemical potential, Q-value, shell and pair effects. The SES strongly influences the beta decay threshold energy and the chemical potential. Thus, it is very important to accurately investigate the beta decay neutrino energy loss in the SES.

Our previous studies [31, 32] demonstrated that the SES affects the beta decay rates and neutrino cooling to a great degree. However, these studies neglected the SES effect on the chemical potential in the beta decay. Toki et al. [33] have calculated β-transition rates for the URCA process using the $s-d$ shell model. They considered many β–transitions, including excited states necessary for the electron capture and β–decay at high density and high temperature. Recently, Suzuki et al. [34] also evaluated the electron capture and β-decay rates based on the $s-d$ shell model for electron-degenerate O – Ne – Mg cores with initial masses of 8–10 $M_{\odot}$($M_{\odot}$ denotes the solar mass).

Our studies differ from these works [33, 34] in discussing the SES effects on the beta decay and neutrino cooling. First, these works discussed the weak interaction rates for some O – Ne – Mg nuclei based on the $s-d$ model theory, whereas in the present paper, we focus on the some iron group nuclei and discuss the beta decay re-

Received 3 December 2018, Revised 26 March 2019, Published online 7 May 2019

* Supported in part by the National Natural Science Foundation of China (11565020), the Counterpart Foundation of Sanya (2016PT43), the Special Foundation of Science and Technology Cooperation for Advanced Academy and Regional of Sanya (2016YD28), the Scientific Research Starting Foundation for 515 Talented Project of Hainan Tropical Ocean University (RHDRC201701) and the Natural Science Foundation of Hainan Province (118MS071)

1) E-mail: syjjliu68@qzu.edu.cn

2) E-mail: liudongmei72@126.com

action based on the $p-f$ shell model. Second, there are two Coulomb effects due to SES: one is the screening effect of the electrons, and the other is the change of threshold energy due to the change of chemical potential of the ions. Nuclear reaction rates in dense plasmas depend in a number of crucial ways on their thermodynamic functions. Enhancement due to internuclear multiparticle processes is described in terms of increments in the excess of chemical potentials before and after nuclear reactions. Screening distances of internuclear potentials are likewise described by the compressibility of the electron gas. These studies discussed the effect caused by the correction of the chemical potential of the nucleus due to the interactions between nucleus and electron background based on the Ichimaru model [35]. We discussed the SES problem based on the Potekhin model [36, 37]. The polarizable electron background is calculated for ion charges $Z=26$ and a wide domain of plasma parameters ranging from the Debye limit to the crystallization point. Our calculations are based on the linear-response theory for the electron-ion interaction, including the local-field corrections in the electronic dielectric function. Finally, their studies only discussed the effect of SES on the weak interaction reaction and the neutrino cooling by considering the corrections of the Q-value, electron chemical potential, and the electron energy. Following the study from Ref. [38], we calculate the half-lives of some iron group nuclei of β^--decay, taking into account shell and pair effects. Based on the ion ball screening model (IBSM) (i.e., SES model(I)) [10], and the linear-response theory model (LRTM)(i.e., SES model(II)) [36, 37, 39], we calculate the screening corrections to AELR by β^- decay for ^{56}V, ^{56}Cr, ^{56}Mn, ^{56}Fe, ^{56}Co, and ^{56}Ni. We also discuss and compare the results of model (I) with those of the SES model (II).

The SES model (I) is mainly focused on the screening electrostatic potential per electron under the Wigner-Seitz approximation and Q-value correction based on the IBSM from Ref. [20]. The SES model (II) is mainly focused on the linear response theory by considering the effect of the SES on the Q-value and Coulomb chemical potential due to the change of Coulomb free energy (see Refs. [36, 37, 39] for a detailed discussion)

We organize this paper as follows. In Section 2, we study the beta decay AELR and the half-lives in the absence of SES. In Section 3, we discuss the screening potential, and the screening corrections to the Q-value and the AELR for the model (I). In Section 4, we discuss the AELR and the screening corrections of the Q-value, the electron chemical potential for the model (II). We analyze the influence of SES on the AELR. Our results and discussions are provided in Section 5. In Section 6, we present our conclusions.

2 Antineutrino energy loss by beta decay in the absence of SES

In the absence of SES, the AELR by β^- decay at temperature T is given by (e.g., Refs. [1-4])

$$\lambda^0_{\rm AELR}=\ln 2\sum\frac{(2J_i+1)\mathrm{e}^{\frac{-E_i}{k_BT}}}{G(Z,A,T)}\sum_f\frac{\xi(\rho,T,Y_e,Q_{ij})}{ft_{ij}}, \quad (1)$$

where $G(Z,A,T)$ is the nuclear partition function; Z,A,T are the electric charge on nucleus, mass number, and the temperature, respectively; ft_{ij} is the comparative half-life connecting states of i and j; k_B is the Boltzmann constant, and J_i is the spin. Q_{ij} is the nuclear energy difference between the states of i and j, respectively. $Q_{00}=M_pc^2-M_dc^2$, M_p and M_d are the masses of the parent nucleus and the daughter nucleus, respectively, E_i and E_j, are the excitation energies of the i th and j th nuclear state. The $\xi(\rho,T,Y_e,Q_{ij})$ in Eq.(1) for the AELR by β^- decay is

$$\xi(\rho,T,Y_e,Q_{ij})=\frac{c^3}{(m_ec^2)^5}\int_1^{Q_{ij}}\mathrm{d}\varepsilon_e\varepsilon_e(\varepsilon_e^2-1)^{1/2}\times(Q_{ij}-\varepsilon_e)^3\frac{F(Z+1,\varepsilon_e)}{1+\exp[(U_F-\varepsilon_e)/k_BT]}, \quad (2)$$

where $F(Z+1,\varepsilon_e)$ is the Coulomb wave correction. ε_e is the electron energy, and U_F,m_e,p are the electron's chemical potential, mass, and momentum, respectively.

In the pre-collapse phase, the electron chemical potential is given by [30]

$$U_F=1.11(\rho_7Y_e)^{1/3}\left[1+\left(\frac{\pi}{1.11}\right)\frac{(k_BT)^2}{(\rho_7Y_e)^{2/3}}\right]^{-1/3}\ \text{MeV}. \quad (3)$$

Ref. [38] discussed the beta-decay half-lives of the r-process nuclei with a consideration of the shell and pair effects, as well as the decay energy Q. Then, the comparative half-life ft_{ij} is written as

$$\ln(ft_{ij})=a_1+\left(\alpha^2Z^2-5+a_2\frac{N-Z}{A}\right)\ln(Q_{if}-a_3\delta)+(a_4\alpha^2Z^2)+\frac{1}{3}\alpha^2Z^2\ln(A)-\alpha Z\pi+S(N,Z), \quad (4)$$

where the fine structure constant $\alpha=1/137$, and $\delta=(-1)^N+(-1)^Z$. Taking into account the pairing effects on Q-values, and the shell effects, the correction factor $S(N,Z)$ is written as [28]

$$\begin{aligned}S(N,Z)=&a_5\exp(-((N-28)^2+(N-20)^2)/12)\\&+a_6\exp(-((N-50)^2+(N-38)^2)/43)\\&+a_7\exp(-((N-82)^2+(N-50)^2)/13)\\&+a_8\exp(-((N-82)^2+(N-58)^2)/24)\\&+a_9\exp(-((N-110)^2+(N-70)^2)/244),\end{aligned} \quad (5)$$

where $a_i(i=1,2,3,...9)$ are 11.09, 1.07, −0.935, −5.398, 3.016, 3.879, 1.322, 6.030, 1.669, respectively, in Eqs. (4–5).

3 Antineutrino energy loss by beta decay with SES for model (I)

The free electron gas is relativistic and completely degenerated in a supernova. The incoming (outgoing) electrons in the EC (beta decay) process mainly originate from near the Fermi surface. Their Fermi energy is $E_F > 1$ MeV when the density is $\rho > 10^7$g/cm^3. The screening electrostatic potential in the pre-supernova core is much stronger than the one in the main sequence stars. Based on the ion ball screening model (IBSM), the screening electrostatic potential per electron under the Wigner-Seitz approximation is determined by [20]

$$D_1 = 1.784\times10^{-5}\left(\frac{Z^{5/3}}{AY_e^{2/3}}\right)\rho^{1/3}\ \ \text{MeV}. \tag{6}$$

Due to the SES effect, the beta decay Q-value will change by a factor of (e.g., Refs. [1, 2])

$$\Delta Q \approx 2.940\times10^{-5}Z^{2/3}(\rho Y_e)^{1/3}\ \ \text{MeV}. \tag{7}$$

Therefore, the Q-value of beta decay changes from Q_{if} to $Q^s_{if}(\mathrm{I}) = Q_{if} - \Delta Q$.

We can not neglect the SES influence at high density, as the screening energy is high. The electron energy will change from ε_e to $\varepsilon^s_e(\mathrm{I}) = \varepsilon_e + D_1$ in the beta decay. Due to SES, the threshold energy for the beta decay decreases from Q_{if} to $Q^s_{if}(\mathrm{I}) = Q_{if} - \Delta Q$. The $\xi(\rho,T,Y_e,Q_{ij})$ in Eq. (2) is also replaced by $\xi^s(\rho,T,Y_e,Q^s_{ij}(\mathrm{I}))$, given by

$$\begin{aligned}\xi^s(\rho,T,Y_e,Q^s_{ij})(\mathrm{I}) =& \frac{c^3}{(m_ec^2)^5}\int_{1+D_1}^{Q^s_{ij}(\mathrm{II})+D_1}\mathrm{d}\varepsilon^s_e\varepsilon^s_e\\ &\times((\varepsilon^s_e)^2-1)^{1/2}(Q^s_{ij}-\varepsilon^s_e)^3\\ &\times\frac{F(Z+1,\varepsilon^s_e)}{1+\exp[(U_F-\varepsilon^s_e)/k_BT]}.\end{aligned} \tag{8}$$

Therefore, according to Eq. (1), the AELR by beta decay in the SES is given by

$$\lambda^s_{\mathrm{AELR}}(\mathrm{I}) = \ln 2\sum\frac{(2J_i+1)\mathrm{e}^{\frac{-E_i}{k_BT}}}{G(Z,A,T)}\sum_f\frac{\xi^s(\rho,T,Y_e,Q^s_{ij})}{ft^s_{ij}}, \tag{9}$$

where ft^s_{ij} is the half-life in the SES

$$\begin{aligned}\ln(ft^s_{ij})(\mathrm{I}) =& a_1+\left(\alpha^2Z^2-5+a_2\frac{N-Z}{A}\right)\ln(Q^s_{if}-a_3\delta)\\ &+(a_4\alpha^2Z^2)+\frac{1}{3}\alpha^2Z^2\ln(A)-\alpha Z\pi+S(N,Z).\end{aligned} \tag{10}$$

4 Antineutrino energy loss by beta decaywith SES for model (II)

Itoh et al. [40] investigated the influence of the screening potential on EC by the linear-response theory model (LRTM). The condition is

$$T \ll T_F = 5.930\times10^9\left\{\left[1+1.018\left(\frac{Z}{A}\right)^{2/3}(10\rho_7)^{2/3}\right]^{1/2}-1\right\}, \tag{11}$$

where T_{F} is the electron Fermi temperature, and ρ_7 is the mass density in units of 10^7g/cm^3.

The static longitudinal dielectric function has been discussed by Jancovici et al. [41] for relativistic degenerate of electron fluid. Because of the SES effect, the electron potential energy is given by

$$V(r) = -\frac{Ze^2(2k_{\mathrm{F}})}{2k_{\mathrm{F}}r}\frac{2}{\pi}\int_0^\infty\frac{\sin[(2k_{\mathrm{F}}r)]q}{q\epsilon(q,0)}\mathrm{d}q, \tag{12}$$

where k_{F} is the electron Fermi wave-number, and $\epsilon(q,0)$ is Jancovici's static longitudinal dielectric function.

According to the linear response theory, the screening potential is determined by

$$D_2 = 7.525\times10^{-3}Z\left(\frac{10Z\rho_7}{A}\right)^{\frac{1}{3}}J(r_s,R)\ (\mathrm{MeV}), \tag{13}$$

where the parameters $J(r_s,R)$, r_s, and R are given in Ref. [40]. Eq. (13) and $10^{-5}\leqslant r_s\leqslant10^{-1}, 0\leqslant R\leqslant50$ are fulfilled in the pre-supernova environment.

It is well known that the SES also plays a key role in determining the thermodynamical properties at high density plasma surrounding [42]. When one includes the contribution of the SES, the chemical potential for nuclei is given by

$$U^s_F = U^0_F + U_{iC}, \tag{14}$$

where U^0_F is the chemical potential in the absence of Coulomb effects, and ΔU_F is the contribution to the chemical potential due to the interaction of the nuclei i with the electron background.

Because the stellar core can comprise multi-component plasma, all the thermodynamic quantities are computed as the sum of the individual quantities for each species. If one further assumes that the electron distribution is not affected by the presence of the nuclear charges (uniform background approximation), the correction from Coulomb chemical potential of the nuclei i is given by [32]

$$U_{iC} = kTf_C(\Gamma_i), \tag{15}$$

where k is Boltzmanns constant, f_C, and $\Gamma_i = Z_i^{5/3}\Gamma_e$ are the Coulomb free energy per ion in units of kT, and the ion-coupling parameter, respectively. $\Gamma_e = e^2/a_ekT$, and $a_e = (3/(4\pi n_e))^{1/3}$ is the electron sphere radius, while n_e depicts the electron number density.

According to the discussions for the Coulomb free energy, we will use the expression of (e.g., [36, 37])

$$f_C(\Gamma) = -\Gamma_e\frac{c_{\mathrm{DH}}\sqrt{\Gamma_e}+ac_{\mathrm{TF}}\Gamma^\gamma_eg_1(r_s)h_1(x)}{1+[b\sqrt{\Gamma_e}+ag_2(r_s)\Gamma_e/r_s]h_2(x)}, \tag{16}$$

where the parameter

$$c_{\rm DH} = \frac{Z}{\sqrt{3}}[(1+Z)^{3/2} - Z^{3/2} - 1], \tag{17}$$

and the parameter $c_{\rm TF}$ determines the screening in the limit of large Γ_e and small r_s, given by

$$c_{\rm TF} = c_\infty Z^{7/3}[1 - Z^{-1/3} + 0.2Z^{-1/2}], \tag{18}$$

where $c_\infty = 0.253$ is consistent with the Thomas-Fermi approximation [20], and the parameters $a = 1.11Z^{0.475}$, $b = 0.2 + 0.078(\ln Z)^2$, and $\nu = 1.16 + 0.08\ln(Z)$. The functions $g_1(r_s)$ and $g_2(r_s)$ are written as

$$g_1(r_s) = 1 + \frac{0.78}{21 + \Gamma_e(Z/r_s)^3}\left(\frac{\Gamma_e}{Z}\right)^{1/2}, \tag{19}$$

and

$$g_2(r_s) = 1 + \frac{Z-1}{9}\left(1 + \frac{1}{0.001Z^2 + 2\Gamma_e}\right)\frac{r_s^3}{1+6r_s^2}, \tag{20}$$

respectively. In Eq. (16), the factor $h_1(x) = [1 + (V_F/c)^6 Z^{-1/3}]^{-1}$, where $x = P_F/(m_e c)$, and P_F, m_e, c are the zero-temperature Fermi momentum of electrons, electron mass, and the speed of light, respectively. Here $V_F = cx/\sqrt{1+x^2}$ is the electron Fermi velocity, and $h_2(x) = (1+x^2)^{-1/2}$ is the relativistic correction that may be omitted when $x \ll 1$.

The Coulomb corrections contribute to changing the threshold energy in beta decay by

$$\Delta Q^s_{if}({\rm II}) = U_C(Z+1) - U_C(Z). \tag{21}$$

Thus, the beta-decay threshold energy becomes

$$Q^s_{if}({\rm II}) = Q^{ss}_{if} = Q_{if} + \Delta Q^s_{if}({\rm II}). \tag{22}$$

Due to the SES, the electron energy increases from ε_e to $\varepsilon^s_e({\rm II}) = \varepsilon^{ss}_e = \varepsilon_e + D$ in beta decay, and the threshold energy decreases from Q_{if} to Q^{ss}_{if}. The chemical potential also changes from U_F to U^s_F, and $\xi(\rho, T, Y_e, Q_{ij})$ is replaced by $\xi^{ss}(\rho, T, Y_e, Q^{ss}_{ij})({\rm II})$ in Eq. (2). Thus, we have

$$\begin{aligned}\xi^{ss}(\rho, T, Y_e, Q^{ss}_{ij})({\rm II}) = &\frac{c^3}{(m_e c^2)^5}\int_{1+D_2}^{Q^{ss}_{ij}+D_2} {\rm d}\varepsilon^{ss}_e \varepsilon^{ss}_e \\ &\times ((\varepsilon^{ss}_e)^2 - 1)^{1/2}(Q^{ss}_{ij} - \varepsilon^{ss}_e)^3 \\ &\times \frac{F(Z+1, \varepsilon^{ss}_e)}{1 + \exp[(U^s_F - \varepsilon^{ss}_e)/k_B T]}.\end{aligned} \tag{23}$$

According to Eq. (1), the AELR by beta decay in the SES is given by

$$\lambda^s_{\rm AELR}({\rm II}) = \ln 2 \sum \frac{(2J_i+1){\rm e}^{\frac{-E_i}{k_B T}}}{G(Z, A, T)} \sum_f \frac{\xi^{ss}(\rho, T, Y_e, Q^{ss}_{ij})}{f t^{ss}_{ij}({\rm II})}, \tag{24}$$

where the half-life $f t^{ss}_{ij}$ in the SES for the model (II) is

$$\begin{aligned}\ln(f t^{ss}_{ij}({\rm II})) = &a_1 + \left(\alpha^2 Z^2 - 5 + a_2\frac{N-Z}{A}\right)\ln(Q^{ss}_{if} - a_3\delta) \\ &+ (a_4\alpha^2 Z^2) + \frac{1}{3}\alpha^2 Z^2 \ln(A) - \alpha Z\pi + S(N, Z).\end{aligned} \tag{25}$$

For the purpose of numerical simulation, we define a SES enhancement factor C, which is expressed as

$$C(i) = \frac{\lambda^s_{\rm AELR}(i)}{\lambda^0_{\rm AELR}} \quad (i = 1, 2), \tag{26}$$

where $i = 1, 2$ correspond to model (I) and model (II), respectively.

5 Numerical results and discussions

Figures 1and 2 show the ratios of $\triangle Q/U_F$ and (D/U_F) as a function of electron density ρ_7 for the model (I). We

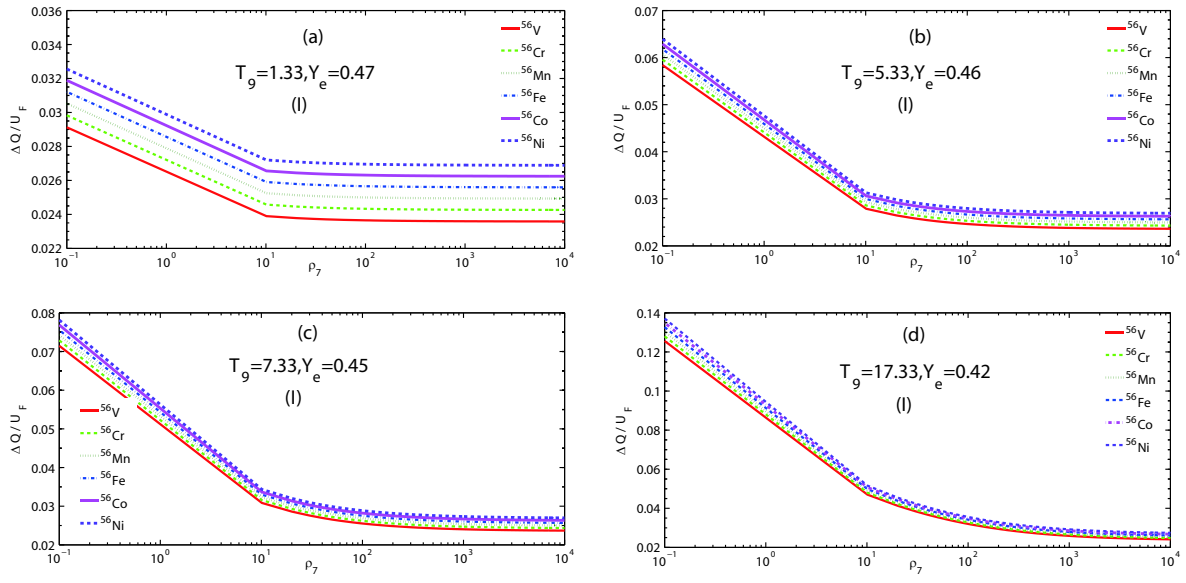

Fig. 1. (color online) $\triangle Q/U_F$ ratio for Q-value correction, and electron Fermi energy as a function of electron density ρ_7 at several typical temperature points for the model (I).

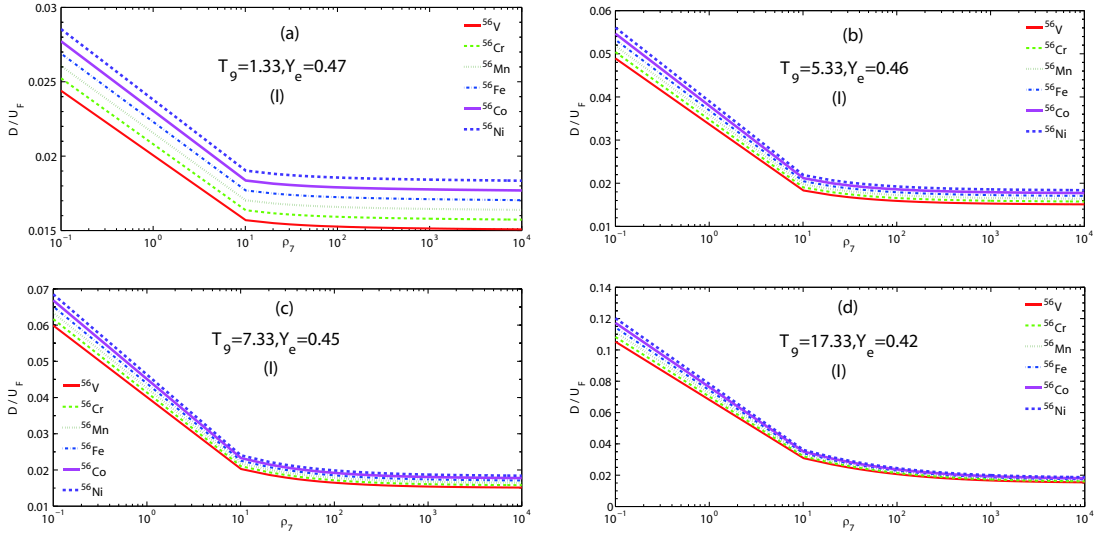

Fig. 2. (color online) D/U_F ratio for screening potential, and electron Fermi energy correction as a function of electron density ρ_7 at several typical temperature points for model (I).

find that $\triangle Q/U_F$, and (D/U_F) decrease significantly as the density increases. However, there is a small effect on $\triangle Q/U_F$ when $\rho_7 > 10$ from Fig. 1(a). Therefore, the beta decay with a low threshold energy is easier to change than that at higher density environment. Figure 1(b) also shows that D/U_F decreases with the density, and that it is hardly related with the matter density when $\rho_7 > 10^2$. For example, D/U_F for ^{56}Fe is 0.03281, 0.02243, 0.01847, 0.01735 at $\rho_7 = 10, 10^2, 10^3, 10^4$, respectively, as shown in Fig. 1. Therefore, the AELR at higher density may be less dependent on the matter density in the SES.

Figures 3 and 4 show the ratios $\triangle Q/U_F^s$, and (D/U_F^s) as a function of the electron density ρ_7 for the model (II). $\triangle Q/U_F^s$, and (D/U_F^s) likewise decrease significantly as the density increases. However, there is little effect on $\triangle D/U_F^s$ when $\rho_7 > 10$ at a relatively higher temperature (e.g., $T_9 \geqslant 5.33$), as shown in Fig. 4. Higher temperatures lead to larger electron energy. The higher the density, the lager the electron chemical potential becomes. According to Eqs. (8, 13–19), the screening effect on D/U_F^s may not strongly depend on the mass density when $\rho_7 > 10$. However, the screening affects $\triangle Q/U_F^s$ significantly, as shown in Fig. 3.

The screening factors C as a function of ρ_7 for the models (I) and (II) are shown in Figs. 5–8 at different densities and temperatures. The effect of the SES on C decreases as the temperature increases for a given density. For example, at $\rho_7 = 10^3$ for model (I), the maximum

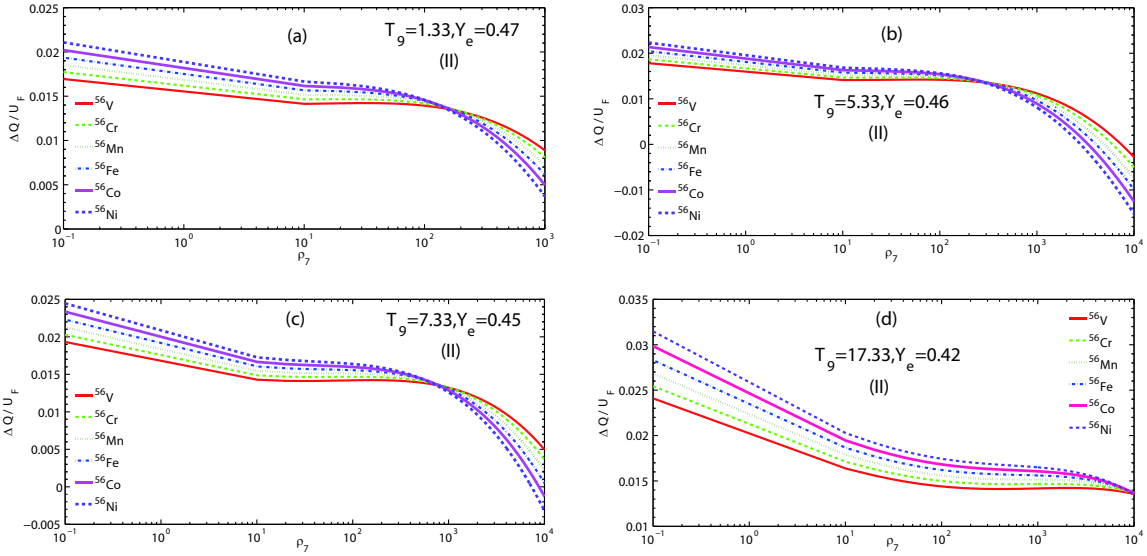

Fig. 3. (color online) $\triangle Q/U_F$ ratio for the corrections of Q-value, and electron Fermi energy as a function of electron density ρ_7 at several typical temperature points for model (II).

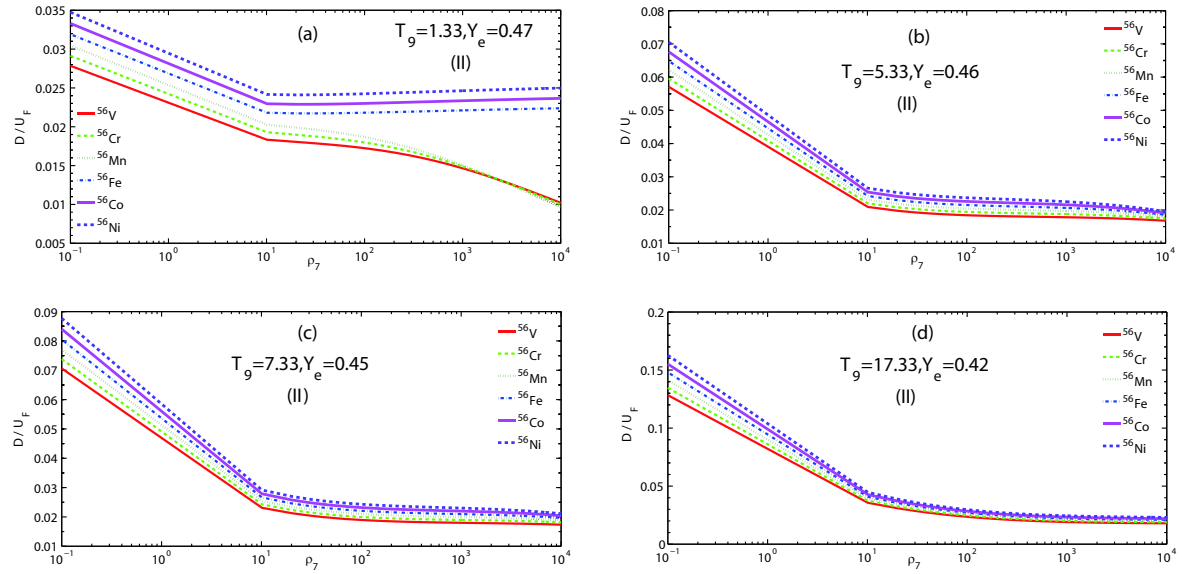

Fig. 4. (color online) D/U_F ratio for the correction of screening potential, and electron Fermi energy as a function of electron density ρ_7 at several typical temperature points for model (II).

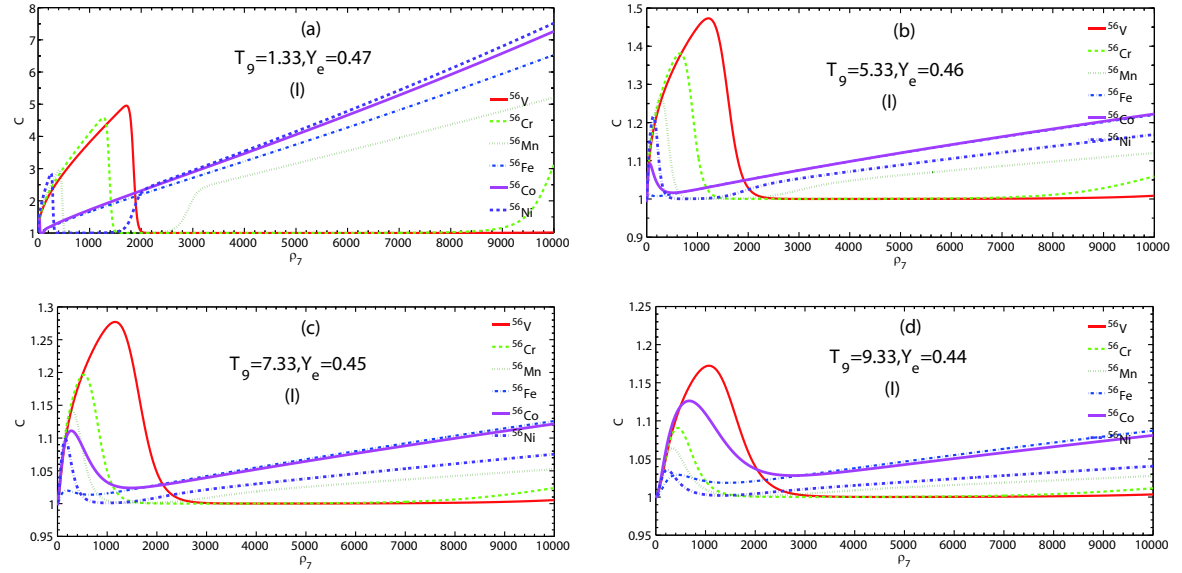

Fig. 5. (color online) Screening enhancement factor C by beta decay of ^{56}V, ^{56}Cr, ^{56}Mn, ^{56}Fe, ^{56}Co, and ^{56}Ni as a function of electron density ρ_7 at relatively lower ($T_9 = 1.33, 5.33$) and medium temperatures ($T_9 = 7.33, 9.33$) for model (I).

C for ^{56}Ni decreases from 7.272 to 1.014, as shown in Fig. 5, and from 33.14 to 4.319 as shown in Fig. 8 for model (II).

At relatively low ($T_9 = 1.33, 5.33$) and moderate temperatures ($T_9 = 7.33, 9.33$), we compare the results of Figs. 5 and 6. Herein, the factor C in model (II) is significantly larger than that of model (I). For example, C for ^{56}V has a value of 4.955 in model (I), whereas it has a value of 651.9 in model (II) at $T_9 = 1.33$. The same conclusions can be derived from Figs. 7 and 8 for higher temperatures. We compare the calculations for Figs. 5 and 6 with those of Figs. 7 and 8 for model (I) and (II). Finally we conclude that the lower the temperature, the smaller the electron kinetic energy becomes. Hence, the SES effect on C and AELR is large.

Judging from the influence of SES on nuclear physics and nuclear structure, the electron screening potential can significantly increase the energy of outgoing electrons during the beta decay process. In addition, the SES can also increase the energy of individual particles, whereas it relatively decreases the threshold needed for beta decay reactions because of the increase in the number of high-energy electrons. Indeed, the SES greatly accelerates the progress of beta decay.

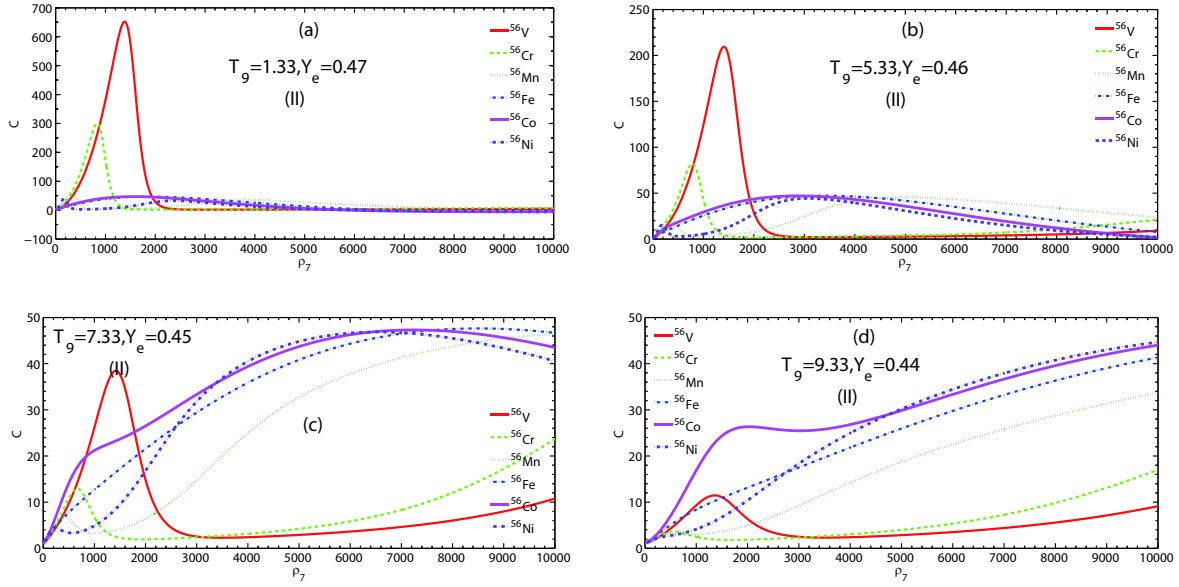

Fig. 6. (color online) Screening enhancement factor C by beta decay of ^{56}V, ^{56}Cr, ^{56}Mn, ^{56}Fe, ^{56}Co, and ^{56}Ni as a function of electron density ρ_7 at relatively lower (T_9 = 1.33, 5.33) and medium temperatures (T_9 = 7.33, 9.33) for model (II).

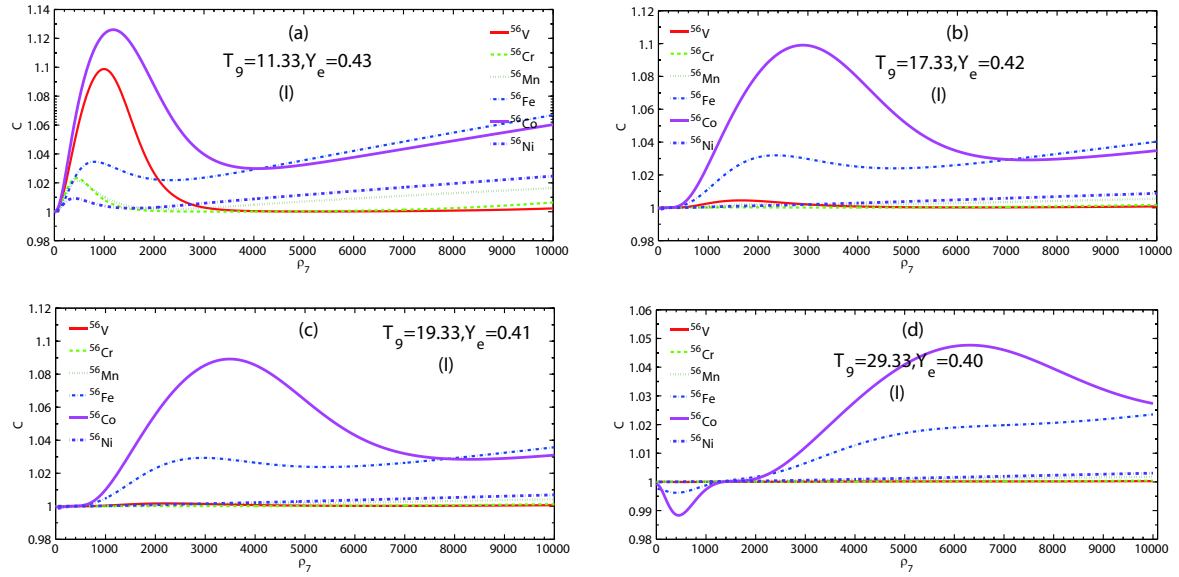

Fig. 7. (color online) Screening enhancement factor C by beta decay of ^{56}V, ^{56}Cr, ^{56}Mn, ^{56}Fe, ^{56}Co, and ^{56}Ni as a function of electron density ρ_7 at relatively high temperature range ($T_9 > 11$) for model (I).

Tables 1–4 show our results in terms of the screening enhancement factor C. The AELR increases greatly due to SES from the information provided by C, especially for model (II). Tables 1 and 2 show the maximum value of the screening factor for ^{56}V, ^{56}Cr, ^{56}Mn, ^{56}Fe, ^{56}Co, and ^{56}Ni at several medium temperatures for model I and II. For example, at $T_9 = 5.33, Y_e = 0.46$ the maximum value of enhancement factor C for ^{56}V, ^{56}Cr, ^{56}Mn, ^{56}Fe, ^{56}Co, and ^{56}Ni are 1.473, 1.381, 1.266, 1.222, 1.223, 1.213 for model (I), whereas they are 209.3, 81.98, 44.58, 43.12, 47.02, 44.26 for model (II), respectively.

The results of C at relatively higher temperatures are presented in Tables 3 and 4. We find that there is small enhancement in C at the higher temperature. For example, the maximum value of the enhancement factor C is 1.099 (e.g., for ^{56}V) in Table 3, whereas is 33.14 (e.g., for ^{56}Ni) in Table 4. This is because the higher the temperature leads to a larger electron energy at a given density. The effect of the SES on beta decay may be weakened due to higher electron energy.

To summarize the above analysis, the C and AELR are both influenced greatly by the SES as the density increases, as seen in Figs. 5-8. This is because the SES has a strong influence on the Q-value of the beta decay. As

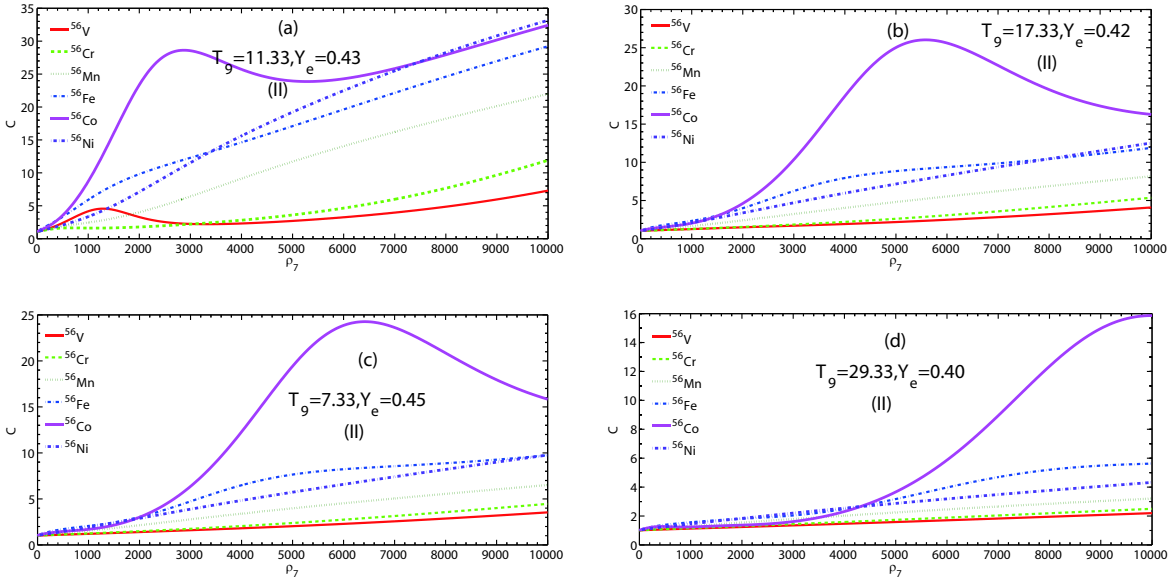

Fig. 8. (color online) Screening enhancement factor C by beta decay of ^{56}V, ^{56}Cr, ^{56}Mn, ^{56}Fe, ^{56}Co, and ^{56}Ni as a function of electron density ρ_7 at relatively high temperature range ($T_9 > 11$) for model (II).

Table 1. Maxima of strong screening enhancement factor C at several typical temperatures within the medium temperature range for model (I).

nuclei	$T_9 = 1.33$, $Y_e = 0.47$		$T_9 = 5.33$, $Y_e = 0.46$		$T_9 = 7.33$, $Y_e = 0.45$		$T_9 = 9.33$, $Y_e = 0.44$	
	ρ_7	C(max)	ρ_7	C(max)	ρ_7	C(max)	ρ_7	C(max)
^{56}V	1712	4.955	1221	1.473	1161	1.277	1071	1.172
^{56}Cr	1271	4.584	650.7	1.381	520.6	1.197	440.5	1.091
^{56}Mn	10000	5.208	260.4	1.266	270.4	1.141	340.4	1.064
^{56}Fe	10000	6.532	10000	1.222	10000	1.126	10000	1.087
^{56}Co	10000	7.257	10000	1.223	10000	1.122	670.8	1.126
^{56}Ni	10000	7.272	150.2	1.213	150.2	1.098	10000	1.041

Table 2. Maxima of strong screening enhancement factor C at several typical temperatures within the medium temperature range for model (II).

nuclei	$T_9 = 1.33$, $Y_e = 0.47$		$T_9 = 5.33$, $Y_e = 0.46$		$T_9 = 7.33$, $Y_e = 0.45$		$T_9 = 9.33$, $Y_e = 0.44$	
	ρ_7	C(max)	ρ_7	C(max)	ρ_7	C(max)	ρ_7	C(max)
^{56}V	1391	651.9	1411	209.3	1422	38.45	1331	11.45
^{56}Cr	810.9	298.2	780.9	81.98	10000	23.66	10000	17.00
^{56}Mn	330.4	64.80	4455	44.58	10000	46.70	10000	33.67
^{56}Fe	1772	46.38	3564	47.12	8509	47.63	10000	41.34
^{56}Co	1452	46.74	2883	47.02	7277	47.31	10000	44.65
^{56}Ni	1703	40.90	3093	44.26	6527	46.85	10000	44.66

the density increases, D/U_F and $\triangle Q/U_F$ decrease. However, they have little relation with mass density when $\rho_7 > 10^2$, as shown in Figs. 1– 4. The AERL is also strongly dependent on the beta decay Q-value. The higher the energy of the outgoing electron, the larger the AERL becomes, in the case where the electron energy is higher than the threshold energy.

For model (I), the SES significantly alters the Q-value, the electron energy, and the half-life for the beta decay. According to Eqs. (7) and (10), due to the Q-value correction, the comparative half-life increases with the increase the Q-value. Because of the interactions among the electrons in plasma, the nuclear binding energy decreases. The effective nuclear Q-value ($Q_{\rm if}$) varies at high density because of the effect of the charge dependence on the binding energy. Based on Eqs. (8) and (9), the beta decay increases due to the SES.

For model (II), we discuss the influence of the SES on

Table 3. Maxima of strong screening enhancement factor C at several typical temperatures in the relatively high temperature range for model (I).

nuclei	$T_9=11.33$, $Y_e=0.43$		$T_9=17.33$, $Y_e=0.42$		$T_9=19.33$, $Y_e=0.41$		$T_9=29.33$, $Y_e=0.40$	
	ρ_7	C(max)	ρ_7	C(max)	ρ_7	C(max)	ρ_7	C(max)
^{56}V	991.1	1.099	1542	1.004	10000	1.001	10000	1.001
^{56}Cr	410.5	1.024	10000	1.002	10000	1.002	10000	1.002
^{56}Mn	460.6	1.021	10000	1.005	10000	1.004	10000	1.003
^{56}Fe	10000	1.067	10000	1.040	10000	1.036	10000	1.023
^{56}Co	1171	1.126	2833	1.099	3413	1.089	6486	1.047
^{56}Ni	10000	1.025	10000	1.009	10000	1.007	10000	1.003

Table 4. Maxima of strong screening enhancement factor C at several typical temperatures in the relatively high temperature range for model (II).

nuclei	$T_9=11.33$, $Y_e=0.43$		$T_9=17.33$, $Y_e=0.42$		$T_9=19.33$, $Y_e=0.41$		$T_9=29.33$, $Y_e=0.40$	
	ρ_7	C(max)	ρ_7	C(max)	ρ_7	C(max)	ρ_7	C(max)
^{56}V	10000	7.286	10000	4.087	10000	3.523	10000	2.196
^{56}Cr	10000	11.86	10000	5.343	10000	4.447	10000	2.492
^{56}Mn	10000	21.91	10000	8.139	10000	6.501	10000	3.205
^{56}Fe	10000	29.16	10000	11.86	10000	9.745	10000	5.622
^{56}Co	2382	32.37	5526	26.01	6326	24.24	10000	15.86
^{56}Ni	10000	33.14	10000	12.49	10000	9.746	10000	4.319

the enhancement factor and AERL by beta decay, by considering the corrections of the Q-value, electron energy, and the half-life, as well as the electron chemical potential. According to Eqs. (13–22, 25), the half-life and electron chemical potential increase due to the the Q-value correction in the SES. The nuclear binding energy also decreases due to interactions with the dense electron gas in the SES. Based on Eqs. (13–24), the beta decay increases greatly due to the SES. Comparison of the results of model (I) with those of model (II), as shown in Figs. 5-8, shows that an improved estimation of the SES for AERL is given in the model (II).

In contrast, the pairing effect and Q-values with the neutron number of the parent nuclei play key roles in the β^- decay reaction. For instance, the half-lives with Q-values are strongly influenced by them. As shown in Fig. 2 of Ref. [36], when the number of neutrons increases, the comparative half-live decreases, whereas the Q-value increases.

The shell and pairing effects are very important in the nuclear structure. Some information on the pairing effects on β^- decay half-lives and Q-values is described by the parameter δ. When the number of nuclear neutrons increases, the beta decay reaction can be more active because of the pairing effect. Thus, the AERL increases.

Because of the quantum effect, the shell effect strongly changes the nuclear structure and influences the β^- decay comparative half-lives. A complete correction of shell effects should include all major shell, as well as sub-shell closures. A reasonable approximation is given by Eq. (4), when we consider the shell effects and pairing effects.

Based on Eqs. (7) and (10) for the model (I) (Eqs. (15–22) and Eq. (25) for the model (II)), the SES influences the Q-value and decay half-lives. From Figs. 1–4, we find that the enhancement factor C rises and falls because of to the shell effects and the pairing effect in the SES, as well as the corrections of the Q-value.

6 Concluding remarks

We investigate the influence of SES on the AELR by beta decay for several iron group nuclei, based on two different SES models. We calculate the screening potential based on IBSM and LRTM. We compare the effect of the SES from two screening models on AELR by considering the corrections of the Q-value, electron chemical potential, and the shell and pair effects. We find that the AELR by beta decay increases by two orders of magnitude, and the enhancement factor can reach 651.9 compared to the case without SES as the density increases in model (II). Meanwhile, this value is 7.272 in model (I) for a given temperature. As the temperature increases, the influence of SES on AELR is weakened. Comparing the results of model (I) with those of model (II), we find that the study of AERL in model (II) may represent an improved estimation.

The AELR by beta decay plays a key role in stellar cooling evolution. Our results may have important consequences for astrophysical applications, and in particular, for the burst mechanism of supernovae explosion and cooling numerical simulations.

References

1 G. M. Fuller, W. A. Fowler, and M. J. Newman, ApJ., **42**: 447 (1980)
2 G. M. Fuller, W. A. Fowler, and M. J. Newman, ApJS., **48**: 279 (1982)
3 M. B. Aufderheide, G. E. Brown, T. T. S. kuo et al, ApJ., **362**: 241 (1990)
4 M. B. Aufderheide, I. Fushikii, S. E. Woosely et al, ApJS., **91**: 389 (1994)
5 K. Langanke and G. Martinez-Pinedo, Phys. Lett. B., **436**: 19 (1998)
6 K. Langanke and G. Martinez-Pinedo, Nuclear Phys. A., **673**: 481 (2000)
7 J. J. Liu and W. M. Gu, ApJS., **224**: 29 (2016)
8 J. J. Liu, MNRAS., **438**: 930 (2014)
9 J. J. Liu, RAA., **16**: 30 (2016)
10 Z. F. Gao, N. Wang, J. P. Yuan et al, ApSS, **332**: 129 (2011a), arXiv:1312.2733
11 Z. F. Gao, Q. H. Peng, N. Wang et al, ApSS, **336**: 427 (2011b), arXiv:1312.2720
12 Z. F. Gao, Q. H. Peng, N. Wang et al, Chinese Physics B, **21**: 057109 (2012a)
13 Z. F. Gao, Q. H. Peng, N. Wang et al, ApSS, **342**: 55 (2012b), arXiv:1312.2679
14 X.-H. Li, Z. F. Gao, X. D. Li et al, IJMPD., **25**: 1650002 (2016), arXiv:1603.00224
15 C. Zhu, Z. F. Gao, X. D. Li et al, MPLA, **31**: 1650070 (2016), arXiv:1603.01933
16 Z. F. Gao, X. D. Li, N. Wang et al, MNRAS, **456**: 55 (2016)
17 Z. F. Gao, H. Shan, W. Wang et al, Astron. Nachr., **338**: 1066 (2017a), arXiv:1709.02734
18 Z. F. Gao, N. Wang, and H. Shan, Astron. Nachr., **338**: 1060 (2017b), arXiv:1709.02186
19 Z. F. Gao, N. Wang, H. Shan et al, ApJ., **849**: 19 (2017c), arXiv:1709.03459
20 E. E. Salpeter, ApJ., **134**: 669 (1961)
21 C. A. Rouse, PhRvA., **4**: 90 (1971)
22 K. Yokoi and M. Yamada, PThPh., **56**: 1781 (1976)
23 K. Langanke, T. D. Shoppa, C. A. Barnes et al, PhLB, **369**: 211 (1996)
24 M. Q. Liu, Y. F. Yuan, and J. Zhang, MNRAS., **400**: 815 (2009)
25 A. Y. Potekhin and G. Chabrier, A&A., **538**: 115 (2012)
26 P. A. Kravchuk and D. G. Yakovlev, PhRvC., **89**: 5802 (2014)
27 Z. Q. Luo and Q. H. Peng, ChA&A, Sci. Sinica A, **39**: 776 (1996)
28 E. Bravo and D. Garcia-Senz, MNRAS., **307**: 984 (1999)
29 J. J. Liu et al, RAA, **17**: 107 (2017)
30 J. J. Liu and D. M. Liu, RAA, **18**: 8 (2018), arXiv:1711.01955
31 J. J. Liu et al, ApSS., **361**: 115 (2018)
32 J. J. Liu and D. M. Liu, NewA., **69**: 69 (2019)
33 H. Toki et al, PhRvC., **88**: 5806 (2013)
34 T. Suzuki, H. Toki, and K. Nomoto, ApJ, **817**: 163 (2016)
35 S. Ichimaru, Rev. Mod. Phys., **65**: 255 (1993)
36 A. Y. Potekhin and G. Chabrier, A&A., **550**: 43 (2013)
37 G. Chabrier and A. Y. Potekhin, PhRvE., **58**: 4941 (1998)
38 Y. Zhou, Z. H. Li, Y. B. Wang et al, Science China Physics, Mechanics & Astronomy., **60**: 082012 (2017)
39 N. Itoh, N. Tomizawa, M. Tamamura et al, ApJ., **579**: 380 (2002)
40 S. A. Bludman and K. A. van Riper, Astrophys. J., **224**: 631 (1978)
41 B. Jancovici, Nuovo Cimento, **25**: 428 (1962)
42 D. G. Yakovlev and D. A. Shalybkov, Sov. Sci. Rev. E., **7**: 311 (1989)